maximum predation, the two densities are close relative to the uncertainty in our estimates. These calculations give the following values: $\lambda = 74.6$; $k = 1.06$; $\hat{b} = 0.14$.

Estimates of predation rates in gypsy moth populations often exceed 99% (ref. 21), which for our parameter values gives deterministic chaos in the combined model in the absence of stochasticity. Because these experimental estimates may be slightly inflated relative to predation rates in natural populations[6], in the figures we use the slightly lower value of $a = 0.967$. For $a = 0.967$ and $\phi = 20$, the model has three equilibria, with the lowest one stable (the intermediate-density equilibrium is always unstable), usefully illustrating the origins of complex dynamics in our model. In fact, as we demonstrate in the Supplementary Information, our results hold for a wide range of parameter values. We estimated the pathogen over-winter survival parameter, ϕ, by first estimating the other parameters, and then adjusting ϕ until the amplitude of density fluctuations in each model matched estimates of the amplitude of density fluctuations derived from the literature[26] (note that the data used to estimate ϕ are densities, and are thus unrelated to the areas defoliated in Figs 1 and 4). Deriving an estimate of the density amplitude from the literature requires that we make some assumption about the detection threshold, the lowest density that can be detected. For detection thresholds of 1–2 egg masses per hectare, our amplitude estimates range from 3.38 to 3.68 orders of magnitude. In this range of amplitude estimates, the inherent stochasticity of the combined model makes it difficult to estimate ϕ with more than one significant digit. Given these uncertainties, we take 3.5 orders of magnitude as our estimate of the observed amplitude, which gives best-fitting values $\phi = 60$ for the combined model and $\phi = 100$ for the host–pathogen model. In Fig. 3, however, we use $\phi = 20$ to illustrate the origins of complex dynamics.

In calculating the statistics in Table 1, we restricted ourselves to time series with at least five outbreaks, to reduce the uncertainty in our estimates of the coefficient of variation of the time between outbreaks. Also, to illustrate irregularity in the inter-outbreak period, we used only species for which the coefficient of variation of the time between outbreaks was at least 0.15. In the case of the gypsy moth (*Lymantria dispar*) and the Douglas-fir tussock moth (*Orgyia pseudotsugata*) the data are spatially referenced. Because the model assumes that populations are well-mixed—so that dispersal does not limit species interactions—for the gypsy moth we used data for particular states, while for the tussock moth we used outbreak regions as in the original source[16]. At these scales, populations are nearly synchronous[27]. Data were periods of outbreaks, except for the following. *Lymantria dispar* data were acres defoliated, and outbreaks were defined as periods in which the area defoliated was more than 1,000 acres, a common definition of an outbreak for defoliation data. *Bupalus piniarius* data were densities, and outbreaks were defined as periods during which the insect's density was greater than its mean density.

Received 10 December 2003; accepted 13 April 2004; doi:10.1038/nature02569.

1. Myers, J. H. Can a general hypothesis explain population cycles of forest Lepidoptera? *Adv. Ecol. Res.* **18,** 179–242 (1988).
2. Liebhold, A. & Kamata, N. Are population cycles and spatial synchrony a universal characteristic of forest insect populations? *Popul. Ecol.* **42,** 205–209 (2000).
3. Varley, G. C., Gradwell, G. R. & Hassell, M. P. *Insect Population Ecology: An Analytical Approach* 135–153 (Blackwell Scientific, Oxford, 1973).
4. Anderson, R. M. & May, R. M. The population-dynamics of micro-parasites and their invertebrate hosts. *Phil. Trans. R. Soc. Lond. B* **291,** 451–524 (1981).
5. Mason, R. R., Torgerson, T. R., Wickman, B. E. & Paul, H. G. Natural regulation of a Douglas-fir tussock moth (Lepidoptera: Lymantriidae) population in the Sierra Nevada. *Environ. Entomol.* **12,** 587–594 (1983).
6. Elkinton, J. S. *et al.* Interactions among gypsy moths, white-footed mice, and acorns. *Ecology* **77,** 2332–2342 (1996).
7. Parry, D., Spence, J. R. & Volney, W. J. A. Response of natural enemies to experimentally increased populations of the forest tent caterpillar, *Malacosoma disstria*. *Ecol. Entomol.* **22,** 97–108 (1997).
8. Klemola, T., Tanhuanpää, M., Korpimäki, E. & Ruohomäki, K. Specialist and generalist natural enemies as an explanation for geographical gradients in population cycles of northern herbivores. *Oikos* **99,** 83–94 (2002).
9. Southwood, T. R. E. & Comins, H. N. A synoptic population model. *J. Anim. Ecol.* **45,** 949–965 (1976).
10. May, R. M. Thresholds and breakpoints in ecosystems with a multiplicity of stable states. *Nature* **269,** 471–477 (1977).
11. Ludwig, D., Jones, D. D. & Holling, C. S. Qualitative analysis of insect outbreak systems: the spruce budworm and forest. *J. Anim. Ecol.* **47,** 315–332 (1978).
12. Rand, D. & Wilson, H. B. Chaotic stochasticity: a ubiquitous source of unpredictability in epidemics. *Proc. R. Soc. Lond. B* **246,** 179–184 (1991).
13. Dennis, B., Desharnais, R. A., Cushing, J. M., Henson, S. M. & Constantino, R. F. Estimating chaos and complex dynamics in an insect population. *Ecol. Monogr.* **71,** 277–303 (2001).
14. Cory, J. S., Hails, R. S. & Sait, S. M. in *The Baculoviruses* (ed. Miller, L. K.) 301–339 (Plenum, New York, 1997).
15. Woods, S. & Elkinton, J. S. Bimodal patterns of mortality from nuclear polyhedrosis virus in gypsy moth (*Lymantria dispar*) populations. *J. Invertebr. Pathol.* **50,** 151–157 (1987).
16. Shepherd, R. F. Evidence of synchronized cycles in outbreak patterns of Douglas-fir tussock moth, *Orgyia pseudotsugata* (McDunnough) (Lepidoptera: Lymantriidae). *Mem. Entomol. Soc. Can.* **146,** 107–121 (1988).
17. Murray, K. D. & Elkinton, J. S. Environmental contamination of egg masses as a major component of transgenerational transmission of gypsy-moth nuclear polyhedrosis virus (LdMNPV). *J. Invertebr. Pathol.* **53,** 324–334 (1989).
18. Dwyer, G., Elkinton, J. S. & Buonaccorsi, J. P. Host heterogeneity in susceptibility and disease dynamics: tests of a mathematical model. *Am. Nat.* **150,** 685–707 (1997).
19. Dwyer, G., Dushoff, J., Elkinton, J. S. & Levin, S. A. Pathogen-driven outbreaks in forest defoliators revisited: building models from experimental data. *Am. Nat.* **156,** 105–120 (2000).
20. Hunter, A. F. in *Population Dynamics: New Approaches and Synthesis* (eds Cappuccino, N. & Price, P. W.) 41–64 (Academic, New York, 1995).
21. Gould, J. R., Elkinton, J. S. & Wallner, W. E. Density-dependent suppression of experimentally created gypsy moth *Lymantria dispar* (Lepidoptera: Lymantriidae) populations by natural enemies. *J. Anim. Ecol.* **59,** 213–233 (1990).
22. Holling, C. S. Some characteristics of simple types of predation and parasitism. *Can. Entomol.* **91,** 293–320 (1959).
23. Kendall, B. E. *et al.* Why do populations cycle? A synthesis of statistical and mechanistic modeling approaches. *Ecology* **80,** 1789–1805 (1999).
24. Bjornstad, O. N. Cycles and synchrony: two historical experiments and one 'experience'. *J. Anim. Ecol.* **69,** 869–873 (2000).
25. Scheffer, S., Carpenter, S., Foley, J. A., Folkes, C. & Walker, B. Catastrophic shifts in ecosystems. *Nature* **413,** 591–596 (2001).
26. Williams, D. W. *et al.* Oak defoliation and population density relationships for the Gypsy Moth (Lepidoptera: Lymantriidae). *J. Econ. Entomol.* **84,** 1508–1514 (1991).
27. Williams, D. W. & Liebhold, A. M. Influence of weather on the synchrony of gypsy moth (Lepidoptera: Lymantriidae) outbreaks in New England. *Environ. Entomol.* **24,** 987–995 (1995).
28. Schwerdtfeger, R. Über die ursachen des massenwechsels der insekten. *Z. Angew. Entomol.* **28,** 254–303 (1941).
29. Ruohomäki, K. *et al.* Causes of cyclicity of *Epirrita autumnata* (Lepidoptera, Geometridae): grandiose theory and tedious practice. *Popul. Ecol.* **42,** 211–223 (2000).
30. Liebhold, A., Kamata, N. & Jacobs, T. Cyclicity and synchrony of historical outbreaks of the beech caterpillar, *Quadricalcarifera punctatella* (Motschulsky) in Japan. *Res. Popul. Ecol.* **38,** 87–94 (1996).

Supplementary Information accompanies the paper on **www.nature.com/nature**.

Acknowledgements We thank O. Bjornstad, P. Turchin and A. Hunter for comments. G.D. and J.D. were supported by grants from the US National Science Foundation. J.D. was also supported by the Andrew W. Mellon Foundation.

Competing interests statement The authors declare that they have no competing financial interests.

Correspondence and requests for materials should be addressed to G.D. (gdwyer@uchicago.edu).

An SCF-like ubiquitin ligase complex that controls presynaptic differentiation

Edward H. Liao[1], Wesley Hung[1], Benjamin Abrams[2] & Mei Zhen[1]

[1]*Department of Medical Genetics and Microbiology, Samuel Lunenfeld Research Institute, University of Toronto, Ontario, Canada M5G 1X5*
[2]*Department of Molecular, Cell and Developmental Biology, University of California, Santa Cruz, California 95064, USA*

During synapse formation, specialized subcellular structures develop at synaptic junctions in a tightly regulated fashion. Cross-signalling initiated by ephrins, Wnts and transforming growth factor-β family members between presynaptic and post-synaptic termini are proposed to govern synapse formation[1–3]. It is not well understood how multiple signals are integrated and regulated by developing synaptic termini to control synaptic differentiation. Here we report the identification of FSN-1, a novel F-box protein that is required in presynaptic neurons for the restriction and/or maturation of synapses in *Caenorhabditis elegans*. Many F-box proteins are target recognition subunits of SCF (Skp, Cullin, F-box) ubiquitin-ligase complexes[4–7]. *fsn-1* functions in the same pathway as *rpm-1*, a gene encoding a large protein with RING finger domains[8,9]. FSN-1 physically associates with RPM-1 and the *C. elegans* homologues of SKP1 and Cullin to form a new type of SCF complex at presynaptic periactive zones. We provide evidence that T10H9.2, which encodes the *C. elegans* receptor tyrosine kinase ALK (anaplastic lymphoma kinase[10]), may be a target or a downstream effector through which FSN-1 stabilizes synapse formation. This neuron-specific, SCF-like complex therefore provides a localized signal to attenuate presynaptic differentiation.

Drosophila and *C. elegans* provide genetic models for uncovering conserved regulatory mechanisms for synapse differentiation[11,12].

Studies indicate that the periactive zone, a presynaptic region that is excluded from active zones and associated vesicles, might regulate synapse growth[13]. Mutations in RPM-1, a *C. elegans* periactive zone protein, cause enlargement in some GABAergic neuromuscular junctions (NMJs) with an excessive number of active zones, whereas other GABAergic NMJs disappear. RPM-1 might restrict the development or promote the maturation of different synapses[8,9]. Its *Drosophila* homologue, HIW, restricts synaptic growth at glutamatergic NMJs[14,15]. The human homologue PAM[16] is expressed in the nervous system. RPM-1/HIW/PAM family proteins contain a Ran-type guanine nucleotide exchange factor domain, multiple RING finger motifs, and a region with unknown structures. RING finger domains are found in many E3 ubiquitin ligases as docking sites for ubiquitin-conjugating enzymes[17], indicating that RPM-1/HIW/PAM might regulate synapse development through a ubiquitin-dependent process. This is supported by the genetic interaction between *hiw* and the deubiquitinating enzyme *fat facets*[18].

To explain the molecular mechanisms by which RPM-1 regulates synapse development, we searched for genes that function in the same pathway. *rpm-1* mutations enhance the locomotion defects of *syd-2(ju37)*, a mutant with mild defects in active-zone morphology[19] (M.Z. and Y. Jin, unpublished observations). Genes that function in the *rpm-1* pathway might also enhance *syd-2*. In a genetic screen for mutations that enhance the locomotion defects of *syd-2*, we recovered *fsn-1*, a mutant with synaptic defects similar to *rpm-1* mutants.

Both *rpm-1*-null and *fsn-1*-null animals have slightly reduced body length and normal locomotion. Examination of the GABAergic NMJs with the use of a synaptic vesicle marker, green fluorescent protein (GFP)-conjugated synaptobrevin[19,20] (*juIs1*, Fig. 1c), in *fsn-1* animals revealed that some vesicle pools are 2–5-fold larger than normal (clusters), whereas some regions lack vesicle pools (gaps) (Fig. 1d). The pan-neural vesicle marker synaptogyrin–GFP (*jsIs219*)[20] revealed similar abnormalities in other synapses in *fsn-1* mutants (Fig. 1a, b). In wild-type animals, a single SYD-2 active-zone punctum is associated with the vesicle pool in most GABAergic NMJs (Fig. 1m). In *fsn-1* animals, the large vesicle clusters contain multiple active-zone puncta (Fig. 1n), indicating that they might be 'overdifferentiated' synapses. SYD-2 protein is absent from the gap areas, confirming that the gaps are devoid of synapses (not shown). The same phenotype was observed in *rpm-1* mutants[9] (Fig. 1o). A postsynaptic GABA receptor marker (UNC-49–GFP)[9] was also clustered in some and missing from other regions of *fsn-1* mutants (Fig. 1j–l). Therefore *fsn-1* synaptic defects include both overdevelopment and underdevelopment of presynaptic and postsynaptic termini, characteristic of the phenotype of *rpm-1* animals.

Consistent with *fsn-1* functioning in the same pathway as *rpm-1* is the observation that *fsn-1;rpm-1* double-null animals display phenotypes similar to that of the *rpm-1* single mutant (Fig. 1d–f). In comparison with the total number of synapses made by the DD motoneurons in wild-type animals (Fig. 1p), *fsn-1*-null animals display a 30% reduction whereas *rpm-1*-null and *rpm-1;fsn-1* double-null animals show a 40% reduction. In addition, *rpm-1* and *fsn-1* mutations synergistically enhance *syd-2* (ref. 19). Both *rpm-1;syd-2* and *fsn-1;syd-2* mutants display a drastic loss of synaptic vesicles in GABAergic NMJs (Fig. 1g–i). Therefore *fsn-1* regulates synaptic development through the *rpm-1* pathway, whereas *rpm-1* has similar but more severe phenotypes in DD motoneurons and in other synapses such as VD and sensory neurons (not shown).

We cloned the *fsn-1* gene by identifying a single open reading frame, C26E6.5, that fully rescues the synaptic defects of *fsn-1* mutants (Supplementary Fig. 1). *fsn-1* encodes a single *C. elegans*

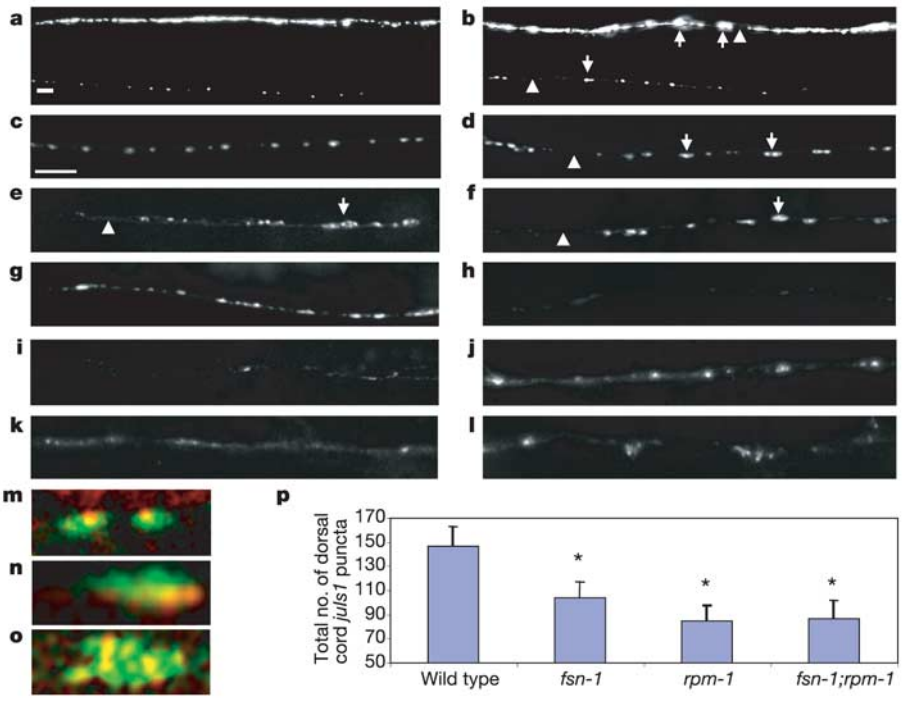

Figure 1 *fsn-1(hp1)* mutants have similar synaptic defects to *rpm-1* animals. **a**, **b**, *jsIs219*, a pan-neural vesicle marker in wild-type (**a**) and *fsn-1* (**b**) animals. *fsn-1* animals have elongated puncta/bulges (arrow) and larger gaps (arrowhead). **c**, **d**, Vesicle marker *juIs1* in GABAergic motoneurons in wild-type (**c**) and *fsn-1* (**d**) animals. Arrows indicate clustered puncta; arrowheads indicate gaps. **e**, **f**, Similar *juIs1* phenotypes in *fsn-1* (**d**), *rpm-1* (**e**) and *fsn-1;rpm-1* (**f**) animals. **g**–**i**, *juIs1* phenotype in *syd-2* (**g**), *fsn-1;syd-2* (**h**) and *rpm-1;syd-2* (**i**) animals. **j**–**l**, GABA receptor marker *oxIs22* in wild-type (**j**) and *fsn-1* animals that show diffusion (**k**) and clustering (**l**) in different regions. **m**, Double labelling of active zone (SYD-2, red) and vesicles (synaptobrevin–GFP, green) in a wild-type GABAergic NMJ[9]. **n**, **o**, Enlarged NMJs contain multiple SYD-2 puncta in *fsn-1* (**n**) and *rpm-1* (**o**)[9] mutants. **p**, Quantification of the total number of *juIs1* puncta by DD motorneurons; $n = 30$. Asterisk, $P < 0.001$ compared with wild type (Kruskal–Wallis test). Error bars show standard deviation. Scale bar, 5 μm.

protein consisting of an F-box domain and a SPRY (for 'spla and ryanodine receptor') domain. Many F-box proteins mediate substrate recognition for SCF ubiquitin-ligase complexes, which contain the invariant components Skp1, Cul1/3 and a RING-finger protein Rbx1[4–7]. SPRY domains mediate protein–protein interactions[21]. The *fsn-1(hp1)* mutation creates a stop codon before the SPRY domain, and behaves as a genetic and a protein null allele (Supplementary Fig. 1). FSN-1 is highly similar to the predicted *Drosophila* and mouse proteins CG4643 and Q8K3B.

We examined FSN-1 localization with anti-FSN-1 antibodies. FSN-1 is expressed specifically in the nervous system in the nerve processes (Fig. 2a, b). At the synapse, FSN-1 is excluded from the active zone because it does not localize with active-zone protein UNC-10 (Fig. 2c, d). It is present at some periactive zones because it resides adjacent to the vesicle region (Fig. 2d) and partly overlaps with RPM-1, which is restricted to periactive zones (Fig. 2e). FSN-1 is also present at non-synaptic, and probably postsynaptic, domains (not shown). At GABAergic NMJs, FSN-1 is absent from the postsynaptic terminal, where GABA receptors localize (Fig. 2f).

Expression of FSN-1 in GABAergic NMJs suggests that it is required in presynaptic neurons. When we expressed FSN-1 cDNA in either GABAergic motoneurons or body wall muscles in *fsn-1*-null animals, only neuronal-FSN-1 expression rescued the defects in GABAergic NMJs. In mosaic animals we found that *fsn-1* is required solely in the neuronal lineage for normal GABAergic NMJs (Supplementary Fig. 2). Therefore FSN-1 is both necessary and sufficient in presynaptic neurons to regulate synapse development in GABAergic NMJs.

Genetic and localization analyses of FSN-1 and RPM-1, and also their predicted structural properties, indicate that they might be components of a neuron-specific E3 complex. We tested this hypothesis biochemically. Because anti-RPM-1 antibody does not work on western analyses, we used an anti-GFP antibody to immunoprecipitate proteins associated with RPM-1 in a transgenic line (*juIs58*)[9] that expresses functional RPM-1–GFP. FSN-1 associated specifically with RPM-1–GFP in *juIs58* animals. We also detected CUL-1 and SKR-1, the *C. elegans* homologues of SCF components Cullin and Skp1 (refs 22, 23) (Fig. 2g, left). Using anti-FSN-1 antibody, we again precipitated a complex containing CUL-1 and SKR-1 from both wild-type and RPM-1–GFP animals (Fig. 2g, right). The precipitation of CUL-1 and SKR-1 is dependent on the presence of FSN-1 and RPM-1 (Fig. 2g), indicating that these four proteins might belong to the same complex. In a yeast two-hybrid system C26E6.5(FSN-1) binds SKR-1, whereas SKR-1 associates with CUL-1 (refs 22, 23). Taken together, these results suggest that a previously unknown SCF protein complex, containing FSN-1, RPM-1, CUL-1 and SKR-1, regulates synapse development at periactive zones.

The FSN-1 complex is unique in that it employs an unusual RING finger subunit, RPM-1. We have determined that Rbx1, the RING finger component in conventional SCF complexes, is unlikely to be present in this complex (Supplementary Fig. 4). Furthermore, the FSN-1 complex depends on RPM-1. RPM-1 is large and consists of several uncharacterized motifs[8,9]. These regions might be used to modulate or extend the function of currently defined SCF complexes.

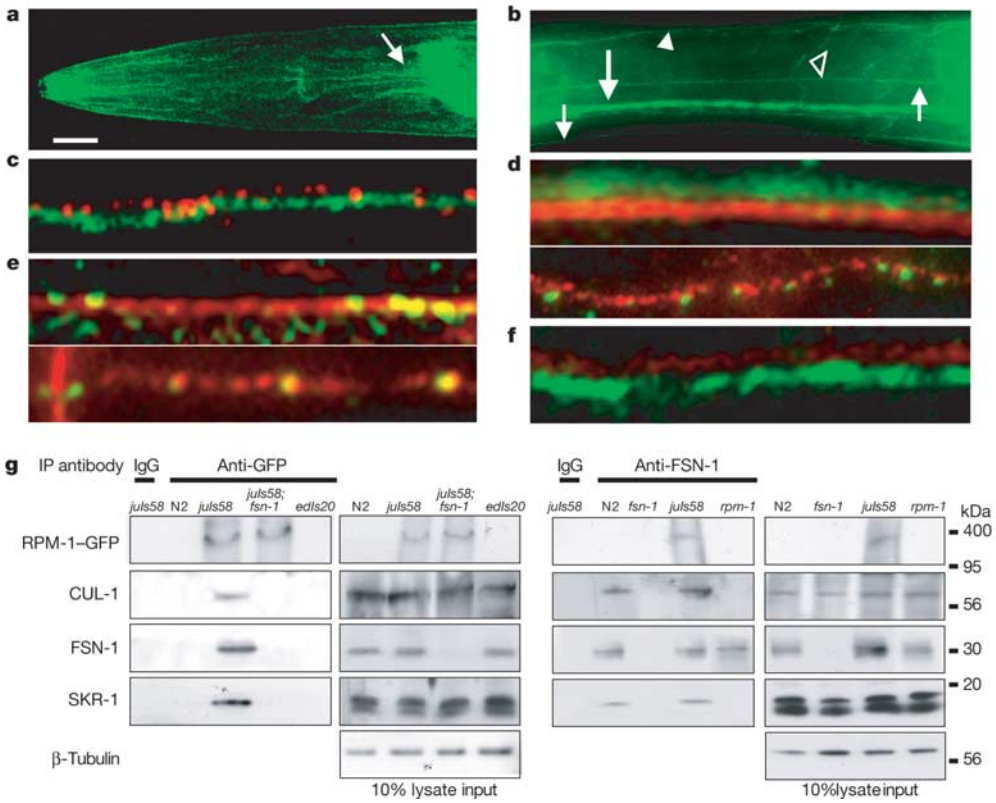

Figure 2 FSN-1 is present at some periactive zones and non-synaptic regions, and forms a complex with RPM-1. **a**, **b**, FSN-1 is expressed throughout the nerve system. **a**, Nerve processes in the head (arrow); **b**, processes in the ventral (long arrow), sub-ventral (short arrow), dorsal (arrowhead) nerve cords and circumferential processes (open arrowhead); **c**–**f**, Immunofluorescent staining for FSN-1 and synaptic components: FSN-1 (green) and active zone (UNC-10, red) (**c**); FSN-1 (red) and vesicles (SNT-1, green) (**d**). Top, the dorsal nerve cord; bottom, the lateral nerve cord where only one layer of synapse is present; FSN-1 (red) and periactive zone protein RPM-1 (green) in the dorsal nerve cord (top) or RPM-1–GFP in the lateral nerve cord (bottom) (**e**); FSN-1 (red) and GABA receptor UNC-49–GFP (green) (**f**). Scale bar, 10 μm (**a**, **b**), 5 μm (**c**, **f**), 0.5 μm (**d**, **e**). **g**, FSN-1 forms a complex with RPM-1, CUL-1 and SKR-1. Left, immunoprecipitation (IP) with anti-GFP antibodies from N2 (wild-type), *juIs58* (RPM-1–GFP)[9], *fsn-1(hp1);juIs58* and *edIs20* (pan-neural GFP expression line) lysates. Right, immunoprecipitation with anti-FSN-1 antibody from N2, *juIs58*, *fsn-1*-null and *rpm-1*-null lysates. The associated proteins were examined with the indicated antibodies.

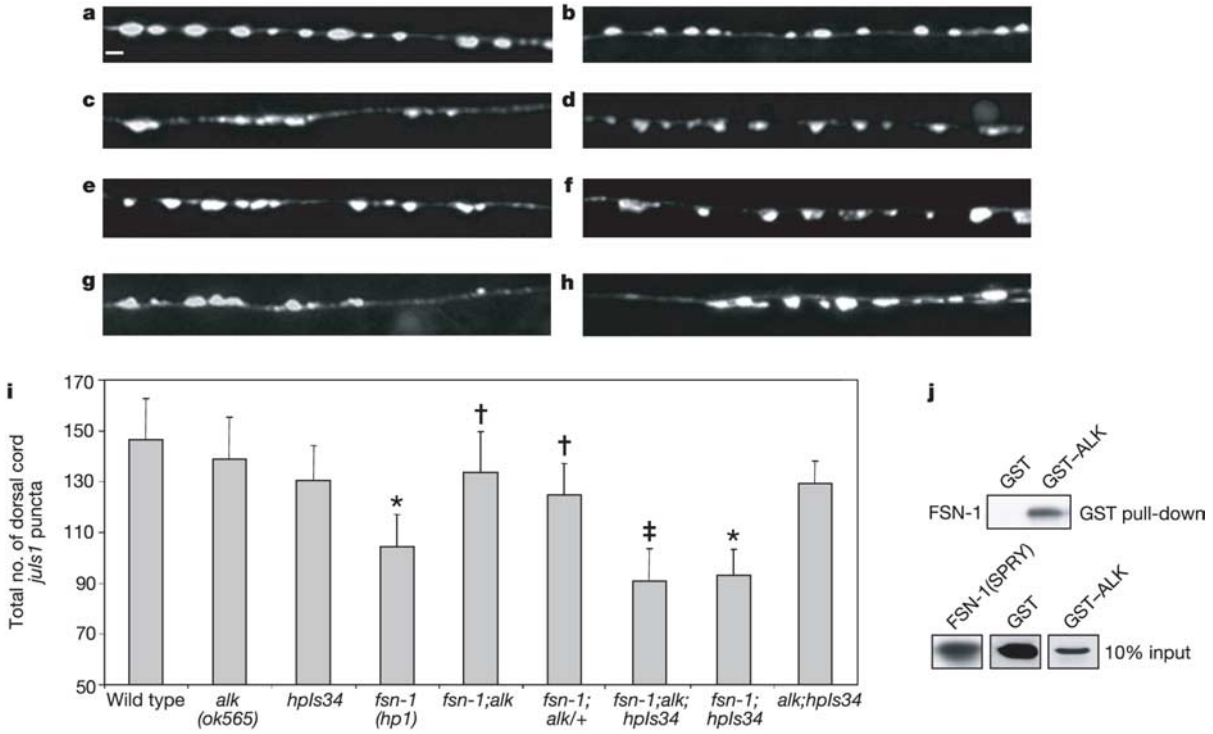

Figure 3 FSN-1 antagonizes the activity of T10H9.2/ALK. **a**–**h**, Morphology of *juls1* marker in wild-type (**a**), *alk(ok565)* (**b**), *fsn-1(hp1)* (**c**), *fsn-1(hp1);alk(ok565)* (**d**), *fsn-1(hp1);ok565/+* (**e**), *hpIs34* (**f**), *fsn-1(hp1);hpIs34* (**g**) and *fsn-1(hp1);alk(ok565);hpIs34* (**h**) animals. *hpIs34* is an integrated ALK–GFP array. Scale bar, 1 μm. **i**, Quantification of total synapse number by DDs; $n = 30$. Asterisk, $P < 0.001$ compared with wild-type; dagger, $P < 0.001$ compared with *fsn-1*; double dagger, $P < 0.001$ compared with *fsn-1;ok565-* (Kruskal–Wallis test). **j**, GST-ALK/T10H9.2 fusion protein associates with the SPRY domain of FSN-1.

To identify FSN-1 targets, we searched for proteins that physically interact with it. We identified T10H9.2, a *C. elegans* receptor tyrosine kinase homologous to a mammalian proto-oncogene anaplastic lymphoma kinase (ALK)[10], as a binding partner of FSN-1. In a precipitation experiment *in vitro*, T10H9.2/ALK intracellular domain binds to the SPRY domain of FSN-1 (Fig. 3j). If FSN-1 regulates synapse development by downregulating a target, the synaptic defects in *fsn-1* mutants might be restored by a simultaneous decrease in the target's activity. *ok565*, a deletion that truncates the entire transmembrane and intracellular domains of ALK protein, causes little abnormality in synapse morphology (Fig. 3a, b), whereas it suppresses the synaptic defects of *fsn-1*. *fsn-1;ok565/+* animals show some improvement in vesicle size and number (Fig. 3c, e), whereas *fsn-1;ok565* animals display restored synapse number and reduced size of abnormal clusters (Fig. 3c, d). Rescue is variable among individuals and is more robust in larvae than in adults, suggesting that ALK is not the only FSN-1 target. To examine the genetic interactions further, we introduced low-copy-number transgenes expressing ALK, or ALK–GFP under its own promoter (*hpIs34*), into *fsn-1;ok565* animals. Although neither array caused significant changes in synapse number in the wild-type (Fig. 3f, i), *fsn-1* (Fig. 3g, i) or *ok565* (Fig. 3i) background, each restored *fsn-1*-like synapse defects in *fsn-1;ok565* animals (Fig. 3h, i). We failed to detect suppression with other *C. elegans* RTK mutants, including Eph/*vab-1*, *egl-15*, *let-23* and *cam-1* (not shown), further supporting the specificity of *ok565*'s effects.

The functional ALK–GFP transgene was used to determine the localization and level of ALK in *fsn-1* and *rpm-1* mutants. In a wild-type background, we detected punctate, low-level expression of ALK–GFP in the nervous system. In head neurons, dim ALK–GFP puncta (red) were associated with active zones (green) (Fig. 4a). In *fsn-1*-null mutants, strong expression of ALK–GFP was present in anterior regions unassociated with active-zone protein (Fig. 4b). In *rpm-1(ju44)*-null mutants, ectopic ALK–GFP staining was also detected, although the level was lower than in *fsn-1* (Fig. 4c). Similarly, in *fsn-1* and *rpm-1* nerve processes in the body we detected more dense and intense ALK–GFP puncta than in wild-type animals (Fig.4d–f). Finally, we showed by western analysis that protein levels of ALK–GFP were elevated in both *fsn-1* (3–4-fold) and *rpm-1* (2–3-fold) mutants, whereas the concentration of another synaptic protein SYD-2 did not increase (Fig. 4g). Therefore the amount and localization of ALK are negatively regulated by FSN-1 and RPM-1. These data suggest that ALK could be a target, or a downstream effector, for FSN-1 in regulating synapse development.

A decrease in *C. elegans* ALK robustly rescues the synaptic morphology defects in *fsn-1* mutants, but only partly rescues *rpm-1* (not shown). It might be caused by the specific *rpm-1* allele. Alternatively, some ALK might be regulated independently through RPM-1. RPM-1 might also function through its other motifs, and this is consistent with a higher degree of synaptic defects in *rpm-1*-null animals.

The t(2;5) translocation in human creates an ectopically expressed constitutively active ALK in lymphocytes, which causes non-Hodgkin's lymphoma[10]. Mammalian ALK is expressed in the developing nervous system, with unknown physiological functions[24]. *Drosophila* ALK is activated by its ligand Jelly belly to specify visceral mesoderm differentiation[25,26]; however, its function in the nervous system remains elusive. We propose that *C. elegans* ALK might inhibit or destabilize synapse differentiation and that this activity is antagonized by FSN-1, directly or indirectly to stabilize synapse development.

Ubiquitination influences the assembly, disassembly and efficacy of synapses[27–30]. We demonstrate the existence of a new SCF-like complex comprising an F-box protein FSN-1, the large RING finger protein RPM-1 and the core SCF subunits CUL-1 and SKR-1 in the

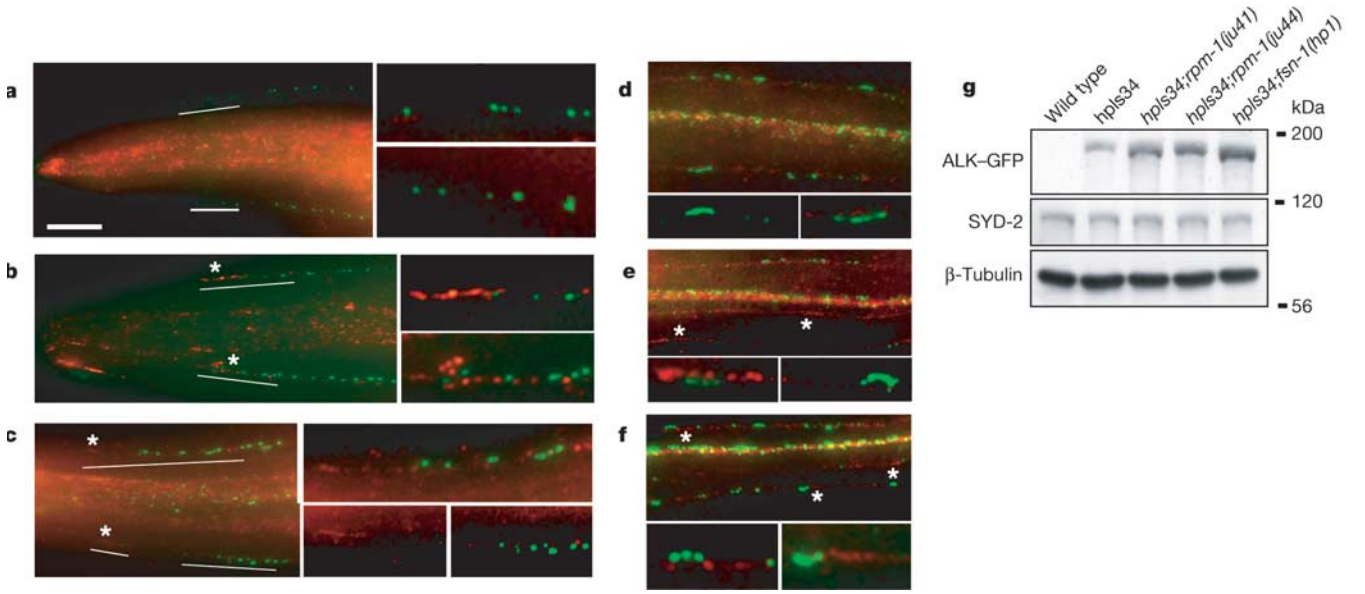

Figure 4 Ectopic and elevated expression of ALK–GFP in *fsn-1* and *rpm-1* mutants. **a**–**f**, *hpIs34* (**a**, **d**), *hpIs34; fsn-1(hp1)* (**b**, **e**) and *hpIs34; rpm-1(ju44)* (**c**, **f**) animals stained with antibodies against GFP (red) and active zone (UNC-10, green). Enlargements of indicated regions in head (**a**–**c**) and body (**d**–**f**) are shown at the right or below the main panel. Asterisks indicate examples of ectopic and more intense ALK–GFP staining. We overexposed images from the brightest *hpIs34* samples. Scale bar, 10 μm. **g**, Western blot analysis on lysates from synchronized larval cultures.

periactive zone of *C. elegans* nervous system. This complex imposes localized regulation of presynaptic differentiation by stabilizing synapse position and extent. It does this in part by downregulating the receptor protein tyrosine kinase ALK. The conserved nature of SCF^{FSN-1} components and its potential effector or target suggests that this machinery operates in all metazoans. □

Methods

Strains and genetics

fsn-1(hp1) was isolated in an enhancer screen from EMS-mutagenized CZ465 *syd-2(ju37)*[19] animals. Paralysed animals were picked from the F_2 progeny. *fsn-1(hp1)* mutation was then outcrossed from the *syd-2* mutation. It was mapped between *mab-21* and *dpy-17* of chromosome III (Supplementary Fig. 1). *hp1* is both a genetic and protein null allele of *fsn-1* (Supplementary Fig. 1). *ok565* was generated by the *C. elegans* Gene Knockout Consortium and backcrossed three times. *hpIs34* line was generated by the simultaneous injection and integration of pJH254 (2 ng μl^{-1}) and RF4 marker (20 ng μl^{-1}) into *juIs1* animals.

Cloning and constructs of *fsn-1*

Cosmids spanning the *fsn-1* mapping region were injected into *fsn-1(hp1);juIs1* animals and scored for rescuing activity. The following constructs were generated from the rescuing cosmid C26E6 and further tested for their rescuing activity: pJH55 removes the 15-kilobase *Nhe*I fragment from C26E6, and it was digested with *Sna*BI, *Pml*I or *Age*I to generate pJH62, pJH63 and pJH125, respectively. pJH122 was generated by inserting the 17-kilobase *Afl*II/*Kpn*I fragment from pJH63 into pSL1180 (Pharmacia). pJH252, the genomic clone for T10H9.2, removes the *Nco*I fragments from F44C4. A GFP fragment was inserted into its *Kpn*I site to create pJH252.

Antibodies and immunofluorescent staining

His_6-tagged full-length or partial (amino acids 85–332) FSN-1 protein were expressed and purified in bacteria. Chicken antibodies were generated against full-length protein (Covance Immunology Service) and affinity-purified against the partial FSN-1. Whole-mount immunofluorescent staining was performed as described except that the reduction was done in 25 mM sodium borate pH 9.5 (ref. 19). Primary antibodies were used at the following concentration/dilution: 30 μg ml^{-1} for anti-FSN-1 antibody, 100 μg ml^{-1} for chicken anti-GFP antibody (Chemicon), 5 μg ml^{-1} for rabbit anti-GFP antibodies (Molecular Probes), 1:250 dilution for rat RPM-1 antibody, 1:2000 dilution for rabbit SNT-1 and 1:10,000 dilution for rabbit UNC-10 antibodies (M. Nonet, Washington University, St Louis).

Co-immunoprecipitation, GST precipitation and western blotting

C. elegans whole lysate was prepared from 0.5 g frozen pellet by sonication in 2 ml lysis buffer (50 mM Hepes pH 7.5, 150 mM NaCl, 10% glycerol, 1% Triton X-100, 1.5 mM $MgCl_2$, 1 mM EGTA, 1 mM dithiothreitol and protease inhibitors). For immunoprecipitation experiments, 250 μg lysate was incubated with 2 μl rabbit GFP antibody (Clontech) or 300 μg ml^{-1} anti-FSN-1 antibody (with 5 μg rabbit anti-chicken IgG as the bridging antibody). Protein A beads (20 μl; Roche) were added and washed with lysis buffer before elution.

For GST precipitation experiments, GST fusion proteins corresponding to T10H9.2 (amino acids 964–1414) were expressed and purified from bacteria. Purified GST fusion protein (10 μg) was pre-bound to glutathione–Sepharose 4B beads and blocked with 1% BSA and 1% milk. It was incubated with 200 μg *C. elegans* lysates or 10 μg purified FSN-1 (amino acids 85–332) protein in binding buffer (20 mM Hepes pH 7.4, 100 mM NaCl, 5 mM dithiothreitol). The beads were washed with binding buffer before elution.

To compare the protein levels of ALK–GFP, synchronized *hpIs34*, *hpIs34;fsn-1(hp1)*, *hpIs34;rpm-1(ju44)* and *hpIs34;rpm-1(ju41)* animals were cultured in liquid and harvested at the same development stages. Equal amounts of total protein from each lysate were used for western analysis. This experiment was repeated five times with five sets of independently prepared culture/lysates. Relative ALK–GFP concentrations were quantified with NIH Image. Final antibody concentrations for western blotting were as follows: anti-FSN-1 (0.9 μg ml^{-1}), rabbit anti-GFP (0.1 μg ml^{-1}; Chemicon), Cul1 (1:1000) and Skp1 (1:1000) (Y. Xiong, University of North Carolina, Chapel Hill).

Fluorescence microscopy and confocal imaging

Images of GFP markers in live *C. elegans* were captured with the Improvision Openlab system (Quorum Technologies Inc.). Confocal images of antibody stainings were obtained with the Zeiss LSM510 system (Zoology Department, University of Toronto).

Received 13 February; accepted 13 May 2004; doi:10.1038/nature02647.
Published online 20 June 2004.

1. Sanes, J. R. & Lichtman, J. W. Development of the vertebrate neuromuscular junction. *Annu. Rev. Neurosci.* **22,** 389–442 (1999).
2. Packard, M., Mathew, D. & Budnik, V. Wnts and TGF beta in synaptogenesis: old friends signaling at new places. *Nature Rev. Neurosci.* **4,** 113–120 (2003).
3. Scheiffele, P. Cell–cell signaling during synapse formation in the CNS. *Annu. Rev. Neurosci.* **26,** 485–508 (2003).
4. Skowyra, D. *et al.* Reconstitution of G1 cyclin ubiquitination with complexes containing SCFGrr1 and Rbx1. *Science* **284,** 662–665 (1999).
5. Tyers, M. & Jorgensen, P. Proteolysis and the cell cycle: with this RING I do thee destroy. *Curr. Opin. Genet. Dev.* **10,** 54–64 (2000).
6. Deshaies, R. J. SCF and Cullin/Ring H2-based ubiquitin ligases. *Dev. Biol.* **15,** 435–467 (1999).
7. Ko, H. W., Jiang, J. & Edery, I. Role for Slimb in the degradation of Drosophila Period protein phosphorylated by Doubletime. *Nature* **420,** 673–678 (2002).
8. Schaefer, A. M., Hadwinger, G. D. & Nonet, M. L. *rpm-1*, a conserved neuronal gene that regulates targeting and synaptogenesis in *C. elegans*. *Neuron* **26,** 345–356 (2000).
9. Zhen, M., Huang, X., Bamber, B. & Jin, Y. Regulation of presynaptic terminal organization by *C. elegans* RPM-1, a putative guanine nucleotide exchanger with a RING-H2 finger domain. *Neuron* **26,** 331–343 (2000).
10. Morris, S. W. *et al.* ALK, the chromosome 2 gene locus altered by the t(2:5) in non-Hodgkin's lymphoma, encodes a novel neural receptor tyrosine kinase that is highly related to leukocyte tyrosine kinase (LTK). *Oncogene* **14,** 2175–2188 (1997).
11. Jin, Y. Synaptogenesis: insights from worm and fly. *Curr. Opin. Neurobiol.* **12,** 71–79 (2002).
12. Broadie, K. S. & Richmond, R. E. Establishing and sculpting the synapse in *Drosophila* and *C. elegans*. *Curr. Opin. Neurobiol.* **12,** 491–498 (2002).

13. Sone, M. *et al.* Synaptic development is controlled in the periactive zones of *Drosophila* synapses. *Development* **127,** 4157–4168 (2000).
14. Wan, H. I. *et al.* Highwire regulates synaptic growth in *Drosophila*. *Neuron* **26,** 313–329 (2000).
15. McCabe, B. D. *et al.* Highwire regulates presynaptic BMP signaling essential for synaptic growth. *Neuron* **41,** 891–905 (2004).
16. Guo, Q., Xie, J., Dang, C. V., Liu, E. T. & Bishop, J. M. Identification of a large Myc-binding protein that contains RCC1-like repeats. *Proc. Natl Acad. Sci. USA* **95,** 9172–9177 (1998).
17. Pickart, C. M. Mechanisms underlying ubiquitination. *Annu. Rev. Biochem.* **70,** 503–533 (2001).
18. DiAntonio, A. *et al.* Ubitiquitination-dependent mechanisms regulate synaptic growth and function. *Nature* **412,** 449–452 (2001).
19. Zhen, M. & Jin, Y. The liprin protein SYD-2 regulates the differentiation of presynaptic termini in *C. elegans*. *Nature* **401,** 371–375 (1999).
20. Nonet, M. L. Visualization of synaptic specializations in live *C. elegans* with synaptic vesicle protein-GFP fusions. *J. Neurosci. Methods* **89,** 33–40 (1999).
21. Wang, D., Li, Z., Messing, E. M. & Wu, G. Activation of Ras/Erk pathway by a novel MET-interacting protein RanBPM. *J. Biol. Chem.* **277,** 36216–36222 (2002).
22. Nayak, S. *et al.* The *Caenorhabditis elegans* Skp1-related gene family: diverse functions in cell proliferation, morphogenesis, and meiosis. *Curr. Biol.* **12,** 277–287 (2002).
23. Yamanaka, A. *et al.* Multiple Skp1-related proteins in *Caenorhabditis elegans*: diverse patterns of interaction with Cullins and F-box proteins. *Curr. Biol.* **12,** 267–275 (2002).
24. Iwahara, T. *et al.* Molecular characterization of ALK, a receptor tyrosine kinase expressed specifically in the nervous system. *Oncogene* **14,** 439–449 (1997).
25. Lee, H. H., Norris, A., Weiss, J. B. & Frash, M. Jelly belly protein activates the receptor tyrosine kinase Alk to specify visceral muscle pioneers. *Nature* **425,** 507–512 (2003).
26. Englund, C. *et al.* Jeb signals through the Alk receptor tyrosine kinase to drive visceral muscle fusion. *Nature* **425,** 512–516 (2003).
27. Speese, S. D., Trotta, N., Rodesch, C. K., Aravamudan, B. & Broadie, K. The ubiquitin proteasome system acutely regulates presynaptic protein turnover and synaptic efficacy. *Curr. Biol.* **13,** 899–910 (2003).
28. Hedge, A. N. & DiAntonio, A. Ubiquitin and the synapse. *Nature Rev. Neurosci.* **3,** 854–861 (2002).
29. Colledge, M. *et al.* Ubiquitination regulates PSD-95 degradation and AMPA receptor surface expression. *Neuron* **40,** 595–607 (2003).
30. Pak, D. T. & Sheng, M. Targeted protein degradation and synapse remodeling by an inducible protein kinase. *Science* **302,** 1368–1373 (2003).

Supplementary Information accompanies the paper on **www.nature.com/nature**.

Acknowledgements We thank the *Caenorhabditis* Genetics Centre, Y. Jin, M. Nonet, B. Bamber, J. Kaplan, I. Greenwald, K.-L. Chow, J. Miwa and D. Pilgrim for *C. elegans* strains; The Gene Knockout Consortium for the *T10H9.2(ok565)* deletion strain; Y. Kohara for EST cDNAs; A. Fire for GFP vectors; the Sanger Institute for cosmids; M. Nonet, M. Tyers and Y. Xiong for antibodies; M. Ailion, Y. Jin, B. Meyer, D. Reiner and J. Thomas for communicating unpublished results; Y. Wang for technical support; members of the Zhen laboratory for discussions; and S. Cordes, J. Culotti, Y. Jin, A. Pawson, J. Rossant, M. Tyers and E. Yeh for comments on the manuscript. M.Z. isolated the *fsn-1(hp1)* mutant when she was a postdoctoral fellow in the laboratory of Y. Jin at UC, Santa Cruz. B.A. is supported by a National Institute of Health grant to Y. Jin. This work was funded by a grant to M.Z. from the Canadian Institute of Health Research, Canada.

Competing interests statement The authors declare that they have no competing financial interests.

Correspondence and requests for materials should be addressed to M.Z. (zhen@mshri.on.ca).

Cell fusion-independent differentiation of neural stem cells to the endothelial lineage

Andrew E. Wurmser[1], Kinichi Nakashima[1,2], Robert G. Summers[1], Nicolas Toni[1], Kevin A. D'Amour[1], Dieter C. Lie[1] & Fred H. Gage[1]

[1]*The Salk Institute, Laboratory of Genetics, 10010 North Torrey Pines Road, La Jolla, California 92037, USA*
[2]*Department of Cell Fate Modulation, Institute of Molecular Embryology and Genetics, Kumamoto University, 2-2-1 Honjo, Kumamoto 860-0811, Japan*

Somatic stem cells have been claimed to possess an unexpectedly broad differentiation potential (referred to here as plasticity) that could be induced by exposing stem cells to the extracellular developmental signals of other lineages in mixed-cell cultures[1–6]. Recently, this and other experimental evidence supporting the existence of stem-cell plasticity have been refuted because stem cells have been shown to adopt the functional features of other lineages by means of cell-fusion-mediated acquisition of lineage-specific determinants (chromosomal DNA) rather than by signal-mediated differentiation[1,2,5,7,8]. In this study we co-cultured mouse neural stem cells (NSCs), which are committed to become neurons and glial cells[9,10], with human endothelial cells, which form the lining of blood vessels[11]. We show that in the presence of endothelial cells six per cent of the NSC population converted to cells that did not express neuronal or glial markers, but instead showed the stable expression of multiple endothelial markers and the capacity to form capillary networks. This was surprising because NSCs and endothelial cells are believed to develop from the ectoderm and mesoderm, respectively. Experiments in which endothelial cells were killed by fixation before co-culture with live NSCs (to prevent cell fusion) and karyotyping analyses, revealed that NSCs had differentiated into endothelial-like cells independently of cell fusion. We conclude that stem-cell plasticity is a true characteristic of NSCs and that the conversion of NSCs to unanticipated cell types can be accomplished without cell fusion.

Previous studies have shown that co-cultured stem cells sometimes take on the characteristics of the cell type with which they are cultured[1–6]. Because NSCs are concentrated at interfaces with the vasculature *in vivo*[12], we reproduced this proximity *in vitro* by co-culturing NSCs with endothelial cells, to determine whether endothelial cells could promote the conversion of NSCs to an endothelial-like cell.

Three clonal lines of NSCs (clones A, B and C), each originating from a single cell, were isolated from mice engineered to constitutively express green fluorescent protein (GFP) in all cell types. Each of our clonally derived, GFP-labelled mouse NSC lines was then co-cultured with a purified population of non-GFP-labelled primary human endothelial cells for 2–5 days (see Methods). All neural and endothelial cells used in these experiments had been passaged only 4–7 times *in vitro*, minimizing the possibility that mutations would occur and affect the outcome of our experiments. To ascertain whether GFP-labelled NSCs could be induced to adopt an endothelial cell phenotype, we probed co-cultures for cells that co-expressed GFP and the endothelial cell adhesion protein, CD146[13,14] (Fig. 1a).

An antibody specific to CD146 recognized human endothelial cells, but not NSCs, neurons or astrocytes (data not shown). In mouse NSC/human endothelial cell co-cultures, non-GFP-expressing human endothelial cells stained for CD146 in a characteristic cell-surface pattern, with the majority of the CD146 signal concentrated at the cell periphery (Fig. 1b). The presence of human endothelial cells induced approximately 6% of the GFP-labelled cells deriving from NSCs to co-label with CD146 in a staining pattern similar to that of human endothelial cells (Fig. 1b). Whereas multi-nucleated cells have previously been observed after cell fusion[5,8], all documented $GFP^+/CD146^+$ cells in our study were uni-nucleate (Fig. 1b).

All of the GFP-labelled NSC clones tested (clones A–C) converted to a CD146-expressing state at a frequency of 5–6.5% after co-culture with human endothelial cells, but not after co-culture with COS7 or NIH3T3 cells under identical conditions (Fig. 1c). The behaviour of these clonal lines was truly representative of the NSC, as a similar percentage (3–9%) of non-clonally purified, low passage (passage 4–7) NSCs expressed CD146 in response to human endothelial cells (data not shown). In the absence of human endothelial cells, mock treatment of NSCs with serum-rich endothelial cell growth medium caused NSC clones A–C to become neurons and astrocytes at frequencies comparable to those previously reported[10] (Fig. 1d). This finding indicates that each of these clonally derived lines behaved as predicted for NSCs and hence that they were free from contamination by non-NSC cell types. Secreted human endothelial cell factors (that is, physical separation of NSCs and human endothelial cells while mixing the respective media)